A COMPARISON OF SOLAR ENERGETIC PARTICLE EVENT TIMESCALES WITH PROPERTIES OF ASSOCIATED CORONAL MASS EJECTIONS

S. W. Kahler
Air Force Research Laboratory, Space Vehicles Directorate, 3550 Aberdeen Avenue, Kirtland AFB,
NM 87117, USA; AFRL.RVB.PA@kirtland.af.mil

ABSTRACT

The dependence of solar energetic proton (SEP) event peak intensities Ip on properties of associated coronal mass ejections (CMEs) has been extensively examined, but the dependence of SEP event timescales is not well known. We define three timescales of 20 MeV SEP events and ask how they are related to speeds v_{CME} or widths W of their associated CMEs observed by LASCO/*SOHO*. The timescales of the EPACT/*Wind* 20 MeV events are TO, the onset time from CME launch to SEP onset; TR, the rise time from onset to half the peak intensity ($0.5I$p); and TD, the duration of the SEP intensity above $0.5I$p. This is a statistical study based on 217 SEP–CME events observed during 1996–2008. The large number of SEP events allows us to examine the SEP–CME relationship in five solar-source longitude ranges. In general, we statistically find that TO declines slightly with v_{CME}, and TR and TD increase with both v_{CME} and W. TO is inversely correlated with log Ip, as expected from a particle background effect. We discuss the implications of this result and find that a background-independent parameter TO+TR also increases with v_{CME} and W. The correlations generally fall below the 98% significance level, but there is a significant correlation between v_{CME} and W which renders interpretation of the timescale results uncertain. We suggest that faster (and wider) CMEs drive shocks and accelerate SEPs over longer times to produce the longer TR and TD SEP timescales.

Key words: acceleration of particles – Sun: coronal mass ejections (CMEs) – Sun: flares – Sun: particle emission

Online-only material: color figures

1. INTRODUCTION

It is widely accepted (Reames 1999, 2013) that there are two classes of solar energetic ($E \geqslant 10$ MeV) particle (SEP) events. The smaller events, called impulsive, are characterized by enhanced abundances of He^3 and Fe/O in the few MeV nuc^{-1} range and are associated with impulsive flares and type III radio bursts. The largest SEP events, called gradual, are produced in coronal and interplanetary shocks driven by coronal mass ejections (CMEs). It is therefore of interest to determine how the gradual SEP event properties are related to the characteristics of the associated CMEs. The SEP event properties of prime interest are those of the peak intensity Ip and energy spectra. The dependence of the occurrence and peak intensities of SEP events on CME properties have been extensively explored using databases of the LASCO/*SOHO* CMEs and the *GOES* $E >$ 10 MeV protons. Recent studies (Reinard & Andrews 2006; Kumar et al. 2009; Hwang et al. 2010; Park et al. 2012) have used the published list of major *GOES* SEP events with peak proton intensities Ip exceeding 10 pfu (1 pfu = 1 p cm^{-2} sr^{-1} s^{-1}), but others (Wang 2006; Gopalswamy et al. 2008) have included weaker ($<$10 pfu) SEP events in their analyses.

Cane et al. (2010) carried out an extensive comparison of SEP events with CMEs over solar cycle 23. Listing 280 SEP events well observed in the 20–30 MeV range with *IMP*-8 and *SOHO* particle detectors, they made flare and CME associations where possible. They looked for systematic variations of a subset of 201 SEP events classified into five groups based on their e/p and Fe/O abundances and observed 1 AU shock associations. There were good correlations between 25 MeV peak proton intensities of all groups, measured within the first 12 hr of the events, and both the listed CME speeds and the CME widths, which they estimated when the CME leading edges were in the LASCO C2 field of view. Their estimated widths replaced where possible

the listed large angle halo widths, usually of 360°. This and other previous work has indicated increasing SEP event occurrence probabilities and Ip with faster and wider CMEs and generally with more western CME source longitudes.

The temporal characteristics of SEP events are also of interest for both space weather forecasting and understanding the SEP injection profiles and propagation characteristics. For example, faster CMEs could begin to accelerate and inject SEPs earlier, producing earlier onsets and perhaps longer rise times. The variations of SEP rise times, taken as time from X-ray flare maximum to SEP maximum at 1 AU, as a function of solar source longitude have been surveyed (Cane et al. 1988; Balch 1999), but within those longitudinal variations the dependence on CME characteristics was not explored until our previous work (Kahler 2005, hereafter K05).

K05 used time profiles of 144 20 MeV proton events observed with the EPACT experiment on the *Wind* spacecraft, which provided a much larger dynamic range of peak SEP intensities than those of the $E >$ 10 MeV *GOES* SEP events. Those 20 MeV SEP events had peak intensities at least a factor of two above background and were observed during the period 1998–2002. For each SEP event the time of projected associated CME onset at the Sun was determined from height–time profiles given in the LASCO CDAW catalog. The three characteristic times of the SEP events were TO, the time from inferred CME launch at 1 $R_{\odot}$ to the time of the 20 MeV SEP onset at *Wind*; TR, the time from SEP onset to the time the intensity reached half the peak value Ip ($0.5I$p); and TD, the time during which the intensity was above $0.5I$p. If an SEP increase occurred with the associated shock passage, then TD was taken only up to the time of the shock.

The three SEP event timescales were compared with the CME speeds v_{CME}, accelerations, widths W, and the solar wind O^{+7}/O^{+6} ratios at 1 AU. The expected longitude dependence

of the timescales (e.g., Cane et al. 1988) was addressed by separating the events into five longitude ranges and looking for significant correlations between SEP and CME parameters in each longitude range. In addition, the median values of the timescales were given for each longitude range, providing a rough guide for space weather forecasting of SEP events.

Several results appeared clear from K05. There was no correlation (at a $\geqslant 98\%$ significance probability) of any SEP timescale with the solar wind O^{+7}/O^{+6} ratios (Kahler 2008), and, with a possible exception of TD for well-connected events, no correlation with CME accelerations. These results would be expected if ambient solar wind particles are not seed particles for the shocks and if CME accelerations are small perturbations of v_{CME}. There was no correlation of TO with v_{CME}, although the median TO was smaller for events in well-connected longitude ranges than for those near the limb, as perhaps expected from earlier studies. TR and TD were significantly correlated with v_{CME} only in the W65°–W90° longitude range. There were large, but not significant, correlations of TD with W for western hemisphere events.

Pan et al. (2011) repeated the analysis of K05 but used the CME ice-cream cone model of Xue et al. (2005) to get more accurate values of v_{CME} and W than the sky-projected values used by K05. They eliminated CMEs with source regions behind the limbs, with irregular structures, or with halos from central meridian sources, which reduced their sample size to 95 events. The model CME speeds resulted in changes in the projected CME onset times and some changes to the TO values, but they retained the TR and TD values of the K05 study. In agreement with K05 they found no correlation of TO with v_{CME} in any longitude region but significant correlations of TR with v_{CME} for the W60°–W90° region and of TD with v_{CME} for both the W30°–W59° and W60°–W90° source regions. Their correlation coefficients (CCs) were substantially enhanced above the corresponding values of K05, an apparent effect of using more accurate values of v_{CME} deduced from the cone model. For the correlations with W Pan et al. (2011) found significant correlations of TR and TD in the W30°–W59° and W60°–W90° source regions, where K05 found only high but not significant correlations. Once again, the cone model seemed to provide the more accurate CME parameters that resulted in better correlations.

This work is an extension of K05 to the full solar cycle from 1996 to 2008. We have added SEP events from 1996 to 1997 and from 2003 to 2008, bringing the new total to 217 SEP events, an increase of 73 events. The previously published 1998–2002 event list is amended with several flare/CME source longitude corrections and event additions and deletions. Besides a check on the results of the previous study, we use the improved statistics to provide comparative plots of median values of each SEP timescale versus v_{CME} or W within each longitude range for an easier overview of the timescale dependences. Based on our earlier results, we do not include here the CME accelerations or the solar wind O^{+7}/O^{+6} values. An important extension of K05 is to explore significant correlations between TO and log Ip and between v_{CME} and W. The goal is to provide a more definitive determination of how 20 MeV SEP timescales depend on the basic properties of CMEs.

2. DATA ANALYSIS

2.1. SEP Event Selection

We follow the same procedure as discussed in detail in K05. We identify all the SEP events in the 18.9–21.9 MeV (hereafter 20 MeV) proton intensity–time profiles from the *Wind*/EPACT instrument and attempt to associate each event with a CME listed in the LASCO (Large Angle Spectroscopic Coronagraph) CDAW catalog. As in K05, we looked at associated Hα and X-ray flare reports and used both the direct and difference 195 Å EIT images superposed on the LASCO movies to locate the solar sources of the CME (eruption region on the disk, at the limb, or behind the limb). The flare location was taken as the source region of the CME, although CME size scales are greater than those of flares, which may lie nearer to the legs than to the centers of the associated CMEs (Harrison 2006). The most frequent flare site, however, is centered under the CME span (Yashiro & Gopalswamy 2009). Some SEP events could not be associated with CMEs, usually because of gaps in LASCO observational coverage.

The description of the SEP parameters TO, TR, and TD and of the CME launch times is given above and in Section 2 of K05. The 20 MeV onset and 0.5Ip times were determined to the nearest half-hour from data plots of that resolution. The parameters v_{CME} and W are measured in the plane of the sky and reported in the CDAW catalog (http://cdaw.gsfc.nasa.gov/CME_list/), although some entries for W here are lower limits in the CDAW catalog. We used the linear height–time fits to deduce the 1 $R_{\odot}$ CME onsets, which can differ by tens of minutes from those based on the quadratic fits that allow CME accelerations.

The new list of 217 20-MeV SEP events is given in Table 1. There we list the date and time of the CME launch, v_{CME}, W, the solar source region, TO, TR, the initial time of 0.5Ip, TD, and Ip. Note that TO+TR equals the time from CME launch to 0.5Ip. Table 1 of K05 has been expanded to include events from the years 1996–1997 and 2003–2008.

All such tables of event associations based on best judgments are provisional and subject to change. Comparisons with other lists of SEP event identifications and associations (Cane et al. 2006, 2010; Desai et al. 2006; Gopalswamy et al. 2004, 2010; J. Park 2011, private communication) yielded discrepancies that were resolved with data sources including SEP plots from the ERNE/*SOHO* experiment, metric and decametric-hectometric (DH) type II burst reports, *SOHO* EIT/LASCO movies, and lists of interplanetary shocks at 1 AU. Event associations from the period 1998–2002 included in Table 1 of K05 have been modified here by several event additions and deletions, modified CME speeds, different CME associations, and changed solar source locations. We added a 2002 event based on observations of the *Mars Odyssey* mission (Krucker et al. 2007). The new list of 217 events in Table 1 includes only SEP events for which the intensity profiles were adequate for making the timing estimates and for which confident solar source longitude and CME associations could be made.

The focus of this study are the gradual SEP events, but our selection criteria do not discriminate between those events and large impulsive SEP events, which can also be associated with CMEs (Kahler et al. 2001). We turn to the survey of impulsive SEP events observed through 2002 September with the Low-Energy Matrix Telescope on the *Wind* spacecraft by Reames & Ng (2004), which overlaps part of our Table 1. Of our 156 SEP events in that time interval, we identify only 6 or 7 matching events in Table 1 of Reames & Ng (2004). If we apply this rate to all of our Table 1, then only ∼5% of the SEP events are impulsive, and our statistical results will generally reflect the properties of gradual SEP events. The impulsive events will, however, lie predominately in well-connected (∼W20°–W80°) longitudes (Cliver & Ling 2007).

Table 1
Properties of CMEs and Associated SEP Events

Date CME	Launch (UT)	v_{CME} (km s^{-1})	W (deg)	Solar Location[a]	TO (hr)	TR (hr)	0.5Ip[b] (UT)	TD (hr)	20 MeV Ip[c]
				1996					
Nov 28	16:10	984	101	bNWL	3.7	1.0	21:00	22.0	0.007
Dec 24	12:10	325	69	bWL	2.3	2.0	16:30	6.0	0.006
				1997					
Apr 1	13:20	312	79	S25E16	6.7	2.0	22:00	41.0	0.002
Apr 7	14:10	878	360	S30E18	1.9	1.5	17:30	25.5	0.009
May 12	4:15	464	360	N21W08	1.7	1.5	7:30	26.5	0.02
May 21	20:00	296	165	N05W12	1.0	1.0	22:00	14.0	0.007
Jul 25	19:50	611	84	N16W54	2.7	0.5	23:00	13.0	0.01
Sep 23	21:45	712	155	S29E26	6.2	1.5	5:30	17.5	0.008
Oct 7	12:30	1271	167	bSWL	1.5	1.5	15:30	13.5	0.009
Nov 3	9:30	352	122	S20W13	2.5	1.5	13:30	NA	0.006
Nov 4	5:20	785	360	S14W33	0.7	2.0	8:00	23.0	0.6
Nov 6	11:35	1556	360	S18W63	0.4	5.0	17:00	20.5	11
Nov 13	20:20	546	288	bSWL	0.8	1.5	23:00	19.0	0.045
				1998					
Jan 26	22:05	399	66	S17W55	2.4	2.5	27 3:00	5.0	0.008
Apr 20	9:55	1863	165	S43W90	1.6	12.5	24:00	36.0	30
Apr 29	16:30	1374	360	S18E20	4.5	14.0	30 11:00	41.5	0.05
May 2	13:20	938	360	S15W15	1.2	2.0	16:30	8.5	2
May 6	8:00	1099	190	S11W65	0.5	1.0	9:30	1.0	4
May 9	3:25	2331	178	S11W90	1.1	5.0	9:30	18.5	0.3
May 27	13:05	878	268	N18W58	1.9	1.0	16:00	11.0	0.002
May 30	22:10	594	63	bSWL	3.8	6.0	31 8:00	8.5	0.003
Jun 4	1:45	1802	360	bNWL	8.7	8.5	19:00	17.0	0.01
Jun 16	18:00	1484	281	S17W90	2.5	8.5	17 5:00	40.0	0.03
Nov 5	20:10	1118	360	N22W18	1.8	11.0	6 9:00	6.0	0.03
Nov 24	2:10	1798	360	S30W90	0.8	4.0	7:00	17.0	0.02
				1999					
Apr 24	13:02	1495	360	bWL	2.0	3.0	18:00	12.0	0.3
May 3	5:50	1584	360	N15E32	12.7	11.5	4 6:00	33.0	0.02
May 9	17:15	615	172	N26W90	1.3	1.0	19:30	4.5	0.04
May 27	10:40	1691	360	bWL	0.7	1.5	12:30	6.5	0.15
Jun 1	18:33	1772	360	bNWL	2.0	8.0	2 4:30	30.5	0.8
Jun 4	6:45	2230	150	N17W69	1.7	1.5	10:00	18.0	0.8
Jun 11	0:20	719	101	bSWL	0.7	1.0	2:00	2.5	0.07
Jun 27	8:15	903	86	N23W25	3.3	2.0	13:30	9.0	0.004
Jun 29[e,f]	5:10	589	164	S15E08	6.8	27.0	30 15:00	37.0	0.002
Jul 25	13:12	1389	360	N38W81	8.3	4.5	26 2:00	29.0	0.0015
Aug 28	17:40	462	245	S26W14	3.3	1.0	22:00	12.5	0.001
Sep 14	7:15	761	122	NWL	0.0	1.0	7:00	17.0	0.0025
Oct 14	8:43	1250	360	N11E32	10.3	9.0	15 5:00	46.0	0.0015
Dec 28	0:25	672	82	N20W56	2.6	2.0	5:00	12.0	0.004
				2000					
Jan 18	17:10	739	360	S19E11	2.8	2.0	22:00	42.0	0.02
Feb 12	4:05	1107	360	N26W23	2.4	1.5	8:00	6.0	0.04
Feb 17	20:05	728	360	S29E07	1.9	2.0	18 0:00	NA	0.02
Feb 18	9:05	890	118	bNWL	0.9	0.5	10:30	2.5	0.4
Mar 2	8:05	776	62	S14W52	1.9	2.0	12:00	8.0	0.01
Mar 3	2:05	841	98	S15W60	1.4	0.5	4:00	3.0	0.01
Apr 4	14:53	1188	360	N16W66	1.6	5.5	22:00	15.5	0.4
Apr 23	12:08	1187	360	bNWL	3.4	4.0	19:30	19.5	0.015
Apr 27	14:00	1110	138	N32W90	2.5	0.5	17:00	10.0	0.003
May 1	10:13	1360	54	N20W54	0.8	0.5	11:30	2.5	0.002
May 4	10:53	1404	170	S17W90	1.1	4.0	16:00	22.0	0.003
May 5	15:18	1594	360	SW90	4.7	10.0	6 6:00	32.0	0.005
May 10	19:10	641	205	N14E20	9.3	3.0	11 7:30	24.5	0.0015
May 15	15:45	1212	165	S24W67	3.7	2.5	21:30	8.5	0.015
Jun 2	20:30	731	112	N16E60	9.0	11.0	4 16:30	30.5	0.0008
Jun 6	15:20	1119	360	N20E14	4.2	21.5	7 17:00	16.0	0.4
Jun 10	16:45	1108	360	N22W38	0.7	0.5	18:00	7.0	1.3
Jun 15	19:25	1081	116	N20W65	1.6	1.0	22:00	15.5	0.0013
Jun 17	2:40	857	133	N22W72	2.8	0.5	6:00	7.5	0.006

Table 1
(Continued)

Date CME	Launch (UT)	v_{CME} (km s^{-1})	W (deg)	Solar Location[a]	TO (hr)	TR (hr)	$0.5I_p$[b] (UT)	TD (hr)	20 MeV I_p[c]
Jun 18	1:40	629	132	N23W85	0.8	1.0	3:30	6.5	0.04
Jun 23	13:50	847	198	N26W72	1.2	1.5	16:30	3.5	0.015
Jun 25	7:42	1617	165	N16W55	3.8	2.5	14:00	17.5	0.03
Jun 28	18:38	1198	134	N20W90	1.9	1.0	21:30	8.5	0.002
Jul 10	21:20	1352	289	N18E49	1.2	4.5	11 3:00	10.5	0.007
Jul 11	12:32	1078	360	N18E27	2.5	1.0	16:00	32.0	0.005
Jul 14	10:25	1674	360	N22W07	1.1	1.5	13:00	26.0	120
Jul 22	11:20	1230	229	N14W56	1.2	1.0	13:30	9.5	0.3
Aug 12	9:38	662	168	bWL	0.9	1.5	12:00	2.0	0.03
Aug 12	14:03	876	161	N13W46	2.0	1.0	17:00	12.0	0.005
Aug 13	6:00	883	154	bWL	11.0	6.5	23:30	20.5	0.007
Sep 7	20:15	422	169	N06W47	2.3	4.5	8 3:00	4.0	0.005
Sep 9	7:40	554	180	N07W67	3.3	1.0	12:00	9.0	0.008
Sep 12	11:45	1550	360	S17W09	1.7	5.5	19:00	26.0	2
Sep 19	8:10	766	76	N14W46	4.8	2.0	15:00	18.0	0.013
Oct 9	23:00	798	360	N01W14	8.0	7.0	14:00	43.0	0.005
Oct 16	6:50	1336	360	bWL	0.7	3.5	11:00	14.5	0.4
Oct 25[f]	8:55	770	360	N10W66	3.6	5.0	17:30	16.5	0.25
Nov 8	22:48	1738	170	N10W77	0.7	3.5	9 3:00	15.0	150
Nov 24[g]	5:08	1289	360	N20W05	1.3	1.5	8:00	NA	0.2
Nov 24	15:10	1245	360	N22W07	0.8	1.0	17:00	8.0	1.5
Nov 25	1:07	2519	360	N07E50	10.9	25.5	26 13:30	15.0	15
Dec 28	11:30	930	360	bNWL	5.0	3.0	19:30	38.5	0.015
				2001					
Jan 5	16:20	828	360	bWL	4.2	2.5	23:00	14.0	0.02
Jan 20	21:08	1507	360	S07E46	6.3	22.0	22 1:30	35.5	0.03
Jan 28	15:45	916	250	S04W59	2.7	1.5	20:00	16.0	0.8
Feb 11	1:10	1183	360	N24W57	2.3	1.5	5:00	15.0	0.009
Feb 26	4:50	851	152	bWL	2.6	2.5	10:00	14.0	0.008
Mar 10	3:30	819	81	N27W42	7.0	3.5	14:00	9.0	0.002
Mar 25	16:20	677	360	N16E25	4.7	22.5	19:30	20.5	0.007
Mar 29	9:52	942	360	N14W12	2.1	4.5	16:30	29.5	0.5
Apr 2	11:00	992	80	N17W65	1.5	1.5	14:00	NA	0.07
Apr 2	21:43	2505	244	N19W72	0.8	9.0	3 7:30	17.5	15
Apr 9	15:32	1192	360	S21W04	2.5	1.0	19:00	NA	0.1
Apr 10	5:22	2411	360	S23W09	3.1	4.5	13:00	23.0	2
Apr 12	10:10	1184	360	S19W43	3.8	2.0	16:00	12.5	0.9
Apr 15	13:30	1199	167	S20W85	0.5	2.5	16:30	11.5	20
Apr 18	2:10	2465	360	bSWL	0.8	4.0	7:00	14.0	5
Apr 26	11:50	1006	360	N17W31	4.7	19.5	27 12:00	14.0	0.02
May 7[f]	11:55	1223	205	bNWL	0.6	3.5	16:00	21.5	0.3
May 20	5:40	546	179	bWL	1.3	3.0	10:00	10.0	0.15
May 29	23:50	2087	216	bEL	18.2	46.5	1 16:30	42.0	0.002
Jun 4	15:30	464	89	N24W59	2.0	0.5	18:00	10.0	0.03
Jun 15	10:10	1090	119	S26E41	0.3	NA	NA	NA	0.002
Jun 15	15:24	1701	360	bSWL	1.1	1.0	17:30	5.5	0.8
Jul 11	23:55	736	148	S20W65	3.1	8.0	12 11:00	9.0	0.001
Jul 19	10:00	1668	166	S08W62	5.0	1.0	16:00	21.0	0.0008
Aug 9[f]	10:20	479	175	N15W18	7.2	6.5	10 0:00	NA	0.03
Aug 9[f]	21:05	909	100	S10E21	9.4	2.5	10 9:00	6.0	0.2
Aug 14	10:40	618	360	N20W20	5.8	3.5	14 20:00	15.0	0.01
Aug 15[f]	23:35	1575	360	bSWL	1.4	1.5	16 2:30	22.5	5
Sep 12	21:20	668	114	S20W75	6.2	1.5	13 5:00	21.0	0.002
Sep 15	10:40	478	130	S21W49	0.8	2.5	14:00	5.5	0.2
Sep 17	8:05	1009	166	S14E04	9.9	3.0	21:00	21.0	0.003
Sep 19	5:45	416	210	bSWL	4.3	1.5	11:30	23.5	0.004
Sep 24	10:20	2402	360	S16E23	1.2	9.5	21:00	21.0	30
Oct 1[f]	5:30	1405	360	S20W84	4.5	5.5	15:30	11.5	8
Oct 9	10:40	973	360	S28E08	8.3	0.5	19:30	24.0	0.03
Oct 19	0:25	558	254	N16W18	2.6	2.0	5:00	NA	0.09
Oct 19	16:20	901	360	N15W29	1.7	0.5	18:30	NA	0.17
Oct 22	14:50	1336	360	S21E18	1.2	3.5	19:30	6.0	0.3
Nov 4	16:10	1810	360	N06W18	1.3	5.5	23:00	25.0	50
Nov 17	4:50	1379	360	S13E42	3.7	20.5	18 5:00	34.0	0.04

Table 1
(Continued)

Date CME	Launch (UT)	v_{CME} (km s^{-1})	W (deg)	Solar Location[a]	TO (hr)	TR (hr)	$0.5Ip$[b] (UT)	TD (hr)	20 MeV Ip[c]
Nov 22	20:15	1443	360	S25W67	0.7	NA	NA	NA	0.5
Nov 22[f]	22:55	1437	360	S15W34	2.6	5.5	23 7:00	24.5	50
Dec 11	9:50	891	121	bSWL	5.7	1.5	17:00	21.0	0.007
Dec 14	8:50	1506	360	N06E90	25.7	16.5	16 3:00	42.0	0.007
Dec 26	5:05	1446	212	N08W54	0.4	2.5	8:00	12.5	10
Dec 28	20:05	2216	360	bSEL	3.9	5.0	29 5:00	17.0	0.7
				2002					
Jan 8[d]	17:47	1794	360	bNEL	32.2	20.0	10 22:00	20.0	1.7
Jan 14[f]	5:33	1492	360	S28W83	3.5	20.0	15 5:00	49.0	0.3
Jan 27	12:10	1136	360	bWL	1.8	0.5	14:30	5.0	0.2
Feb 20	5:55	952	360	N12W72	0.6	0.5	7:00	1.5	0.2
Mar 15	22:24	957	360	S08W03	3.6	6.0	16 8:00	23.0	0.015
Mar 18	2:30	989	360	S10W25	4.5	20.0	19 3:00	10.0	0.7
Mar 22	10:53	1750	360	bWL	2.6	3.0	16:30	17.5	0.03
Apr 11	16:00	540	70	S15W33	3.0	3.0	22:00	7.0	0.015
Apr 14	7:25	757	76	N19W57	6.6	2.0	16:00	15.5	0.005
Apr 17	8:00	1240	360	S14W34	3.0	4.0	15:00	8.0	0.3
Apr 21	1:15	2393	241	S14W84	0.3	5.5	7:00	26.0	20
Apr 30	22:44	1103	195	bWL	2.8	1.0	1 2:30	12.5	0.03
May 20	15:10	553	35	S21E65	1.8	0.5	17:30	5.0	0.005
May 22	3:22	1557	360	S22W53	4.2	13.5	21:00	11.0	1.1
Jul 4	19:45	957	168	bSWL	0.7	2.5	23:00	12.0	0.004
Jul 7[g]	11:04	1423	197	bWL	1.5	3.5	16:00	12.5	0.4
Jul 9	17:43	1076	360	bSWL	4.8	1.0	23:30	21.5	0.03
Jul 15[e]	21:00	1300	188	N19W01	13.0	9.0	16 19:00	17.0	1
Jul 20[d]	20:50	1941	360	bSEL	19.2	15.0	22 07:00	80.0	0.53
Aug 3	18:45	1150	138	S16W76	3.3	1.0	23:00	5.5	0.004
Aug 14	1:50	1309	133	N09W54	0.7	5.5	8:00	8.5	0.25
Aug 16	5:53	1378	152	N07W83	2.1	0.5	8:30	6.5	0.009
Aug 16	12:08	1585	360	S14E20	4.3	5.5	22:00	26.0	0.03
Aug 18	21:15	682	140	S12W19	1.7	0.5	23:30	15.5	0.06
Aug 20	8:10	1099	122	S10W38	0.8	0.5	9:30	8.0	0.025
Aug 22	1:22	998	360	S07W62	1.6	1.0	4:00	16.0	0.4
Aug 24	0:57	1913	360	S02W81	1.6	1.0	3:30	21.0	6
Sep 5	16:32	1748	360	N09E28	7.5	10.5	6 10:30	25.5	0.12
Sep 27	1:08	1502	59	SWL	1.3	0.5	3:00	5.0	0.002
Oct 27[d]	22:45	2115	360	S10E130	28.2	47.0	31 2:00	80.0	0.02
Nov 9	13:10	1838	360	S12W29	2.3	7.0	22:30	9.0	5.5
Nov 24	20:00	1077	360	N17E34	11.0	3.0	25 10:00	33.5	0.0024
Dec 19	21:25	1092	360	N15W09	1.1	1.0	23:30	7.5	0.09
				2003					
Mar 17	19:15	1020	96	S14W39	0.8	1.0	21:00	4.0	0.008
Mar 18	12:10	1601	209	S15W46	1.8	1.0	15:00	9.0	0.006
Apr 7	9:12	719	69	bSWL	0.8	5.0	15:00	26.0	0.005
Apr 21	12:58	784	163	N18E02	3.0	2.0	18:00	31.0	0.006
Apr 23	0:45	916	248	N22W25	1.7	1.0	3:00	19.0	0.015
Apr 24	12:30	609	242	N21W39	1.5	0.5	14:30	1.5	0.013
Apr 25	5:12	806	235	N14E79	15.8	12.	26 9:00	57.0	0.004
May 28	0:20	1366	360	S06W20	1.7	13.0	15:00	21.0	0.2
May 31	2:20	1835	360	S07W65	0.7	1.0	4:00	9.0	0.4
Jun 15	23:40	2053	360	S07E80	8.3	24.0	17 8:00	24	0.003
Aug 19	7:12	412	35	S13W63	1.8	1.5	10:30	4.0	0.004
Aug 19	9:40	468	111	S10W58	NA	NA	14:00	24.0	0.002
Oct 4	18:45	1262	103	bWL	1.2	1.0	21:00	7.5	0.0013
Oct 21	3:30	1484	360	S15E90	24.5	11.0	22 15:00	60.0	0.015
Oct 26	17:40	1537	171	N02W38	0.7	1.0	19:00	14.0	6
Oct 28	11:05	2459	360	S16E08	0.9	1.0	13:00	15.5	20
Oct 29	20:40	2029	360	S15W02	0.8	1.0	22:30	17.5	30
Nov 2	9:05	2036	360	S23WL	1.4	1.0	11:30	5.0	0.5
Nov 2	17:20	2598	360	S14W56	0.7	3.5	21:30	24.0	30
Nov 4	19:40	2657	360	S19W83	1.8	7.0	5 4:30	8.5	6
Nov 18	8:10	1660	360	N00E18	2.3	1.5	13:00	47.0	0.01
Dec 2	10:25	1393	150	S19W89	1.6	3.5	15:30	6.0	1.5

Table 1
(Continued)

Date CME	Launch (UT)	v_{CME} (km s^{-1})	W (deg)	Solar Location[a]	TO (hr)	TR (hr)	$0.5Ip$[b] (UT)	TD (hr)	20 MeV Ip[c]
				2004					
Apr 11	4:00	1645	314	S14W47	1.0	5.0	10:00	12.5	0.4
Jul 5	22:20	1444	360	bSWL	15.7	10.0	6 24:00	87.0	0.002
Jul 12	23:42	409	201	N14W45	1.3	1.5	132:30	14.0	0.02
Jul 25	14:40	1333	360	N08W33	1.3	3.0	19:00	26.0	1.5
Sep 2	23:40	751	360	bWL	3.3	0.5	3:30	32.5	0.002
Sep 12	0:30	1328	360	N04E42	6.5	8.0	15:00	30.0	0.02
Oct 30	6:05	422	360	N14W21	0.4	2.5	9:00	NA	0.03
Nov 1	5:35	925	146	bWL	0.4	1.0	7:00	3.5	2
Nov 7	16:20	1759	360	N09W17	1.7	2.0	20:00	10.0	5
Nov 10	2:10	3387	360	N09W49	3.8	3.0	9:00	19.5	5
Dec 2	23:50	1216	360	N09E03	9.2	6.0	3 15:00	19.5	0.05
				2005					
Jan 15	6:05	2049	360	N11E06	0.9	2.5	9:30	9.5	0.15
Jan 15	22:40	2861	360	N15W05	1.3	11.0	16 11:00	19.0	6
Jan 17	9:05	2094	360	N14W24	2.9	2.0	14:00	31.5	30
Jan 20[h]	6:50	3242	360	N12W58	0.2	1.0	8:00	15.0	20
May 11	18:55	550	360	S10W47	2.1	1.0	22:00	7.0	0.01
May 13	16:50	1689	360	N12E12	0.8	22.0	14 15:30	8.5	5
May 31	13:40	313	134	N12W22	3.3	1.5	18:30	27.5	0.0012
Jun 14	7:00	791	360	N08W45	3.0	1.0	11:00	19.0	0.002
Jul 9	22:00	1540	360	N11W27	3.0	1.5	2:30	6.5	0.03
Jul 12	16:15	523	360	N11W64	2.2	0.5	19:00	3.0	0.003
Jul 13	14:10	1423	360	N11W80	1.8	8.0	14 00:00	9.0	0.2
Jul 14	10:25	2115	360	N11W90	2.6	7.0	20:00	25.0	3
Jul 17	11:15	1527	360	N11W130	2.7	4.0	18:00	12.0	0.7
Aug 22	1:00	1194	360	S08W50	1.0	2.0	4:00	6.0	0.15
Aug 22	17:05	2378	360	S12W60	1.9	5.0	23 00:00	17.0	6
Aug 29	10:40	1600	360	S11W148	2.3	4.0	17:00	28.0	0.03
Aug 31	22:00	1808	360	S11W181	5.0	11.0	1 14:00	23.0	0.035
Sep 13	19:40	1866	360	S09E10	3.7	4.0	14 3:00	26.0	3
				2006					
Jul 6	8:30	911	360	S11W32	1.5	2.0	12:00	21.0	0.05
Aug 16	15:45	888	360	S14W13	4.2	4.0	17 00:00	27.0	0.001
Nov 6	17:35	1994	360	S00E100	2.4	1.0	21:00	33.0	0.002
Dec 13	2:25	1774	360	S06W24	0.6	3.0	6:00	15.0	8
Dec 14	22:00	1042	360	S06W46	2.0	1.0	15 1:00	18.0	0.5
				2007					
May 19	12:55	958	106	N01W05	3.1	1.0	17:00	15.0	0.0015
				2008 none					

Notes.

[a] Solar source latitude and longitude. bWL and bEL are sources behind the west and east limbs.

[b] The time at which the 20 MeV proton intensity reaches about one-half of the peak value. It equals the CME launch time of column (2) + TO + TR. Dates are specified for one-half peak UT only where these differ from CME dates given in column (1).

[c] Peak intensities in protons cm^{-2} s^{-1} sr^{-1} MeV^{-1}.

[d] Additional SEP/CME event.

[e] Different CME.

[f] Different CME source region.

[g] Different CME speed.

[h] CME speed from Gopalswamy et al. (2010).

2.2. SEP Event Statistical Treatment

As in K05, we divide the 217 SEP events into 5 longitude ranges of about 43 events each, listed in the first column of Table 2. A primary goal is to look for SEP/CME correlations by calculating their CCs given in the top (v_{CME}) and middle (W) sections of Table 2. We require a 98% statistical significance, which for 44 cases is CC = 0.35 (Bevington & Robinson 2003).

The signs of the CCs indicate positive or negative correlation trends, and significant CCs are italicized in Table 2.

A scan of the values of TO, TR, and TD of Table 1 shows that each of those values ranges over more than an order of magnitude and that the distributions are skewed toward smaller values. To represent a characteristic value for any set of timescales we use here the median value of each distribution. The few large values of the distributions result in standard deviations

Table 2
Correlation Coefficients of SEP Timescales versus CME Speeds
and Widths and SEP Peak Intensities

SEP Timescale[a]	TO	TR	TD	TO+TR
Longitude (Events)		CME Speeds v_{CME}		
E130°–E06° (41–43)	0.17	0.32	0.04	0.29
E04°–W32° (38–44)	−0.16	0.21	−0.02	0.09
W33°–W60° (43–44)	−0.15	0.23	*0.35*	0.10
W62°–W90° (42–44)	−0.19	*0.41*	*0.42*	0.30
W100°–WL (42)	0.02	0.32	0.08	0.18
		CME Widths W		
W33°–W60°	−0.20	0.25	*0.41*	0.10
W62°–W90°	0.06	*0.36*	0.31	*0.35*
W100°–WL	0.19	0.27	0.32	0.25
		Log 20 MeV Ip		
E130°–E06°	−0.07	0.02	−0.32	−0.03
E04°–W32°	*−0.30*	0.15	−0.04	−0.02
W33°–W60°	*−0.31*	*0.34*	*0.42*	0.10
W62°–W90°	*−0.49*	*0.36*	0.14	0.14
W100°–WL	*−0.40*	−0.07	−0.29	−0.27

Note. [a] Units of hours.

generally comparable to or larger than the medians of TO and TR and comparable to or less than medians of TD. The medians presented here are therefore typical values, but excursions to much larger values do occur. In the following presentations we use median values of both the SEP and CME parameters.

2.3. Correlations of SEP Timescales with CME Speeds v_{CME}

For each SEP timescale and CME parameter comparison, we further subdivided each longitude range into event groups sorted on the CME parameter. For example, for TO and longitude E130°–E06° there are 43 events, and we calculate the median TO for 4 groups sorted by increasing CME speeds, with about 11 events in each group. Those median TO values of each group then constitute the data points of that longitude range shown in the top panel of Figure 1. The other longitude ranges are shown as similar series of four median values plotted at the appropriate TO and v_{CME} medians in the figure, which allows us to compare variations of TO in both v_{CME} and longitude. Similarly, we present the longitude/group medians of TR and TD in the top panels of Figures 2 and 3. Figures 1–3 allow us to look for correlation trends between the SEP timescales and associated v_{CME}, but for statistical significance we need the CCs for each full set of ∼43 events in each longitude range given in Table 2.

The only significant CCs for v_{CME} are those of TR for the W62°–W90° range and TD for both the W33°–W60° and W62°–W90° ranges, but TR correlates positively with v_{CME} for all longitude ranges (Figure 2), consistent with longer SEP injection times from faster CMEs.

The lack of significant correlation of TR for longitudes near the central meridian is consistent with increasing differences between true values and plane-of-sky measurements of v_{CME} (Burkepile et al. 2004). Consistent with this interpretation is the result that the TR CC, as well as the median v_{CME} is lowest for the most central longitude range of E04°–W32°. The CCs of TO and TD are only suggestive of earlier SEP onsets and longer durations with faster CMEs, shown in the longitude groups of Figures 1 and 3.

2.4. Correlations of SEP Times with CME Widths W

For comparison with CME widths W, we use only the three most western longitude ranges, for which the observed W is
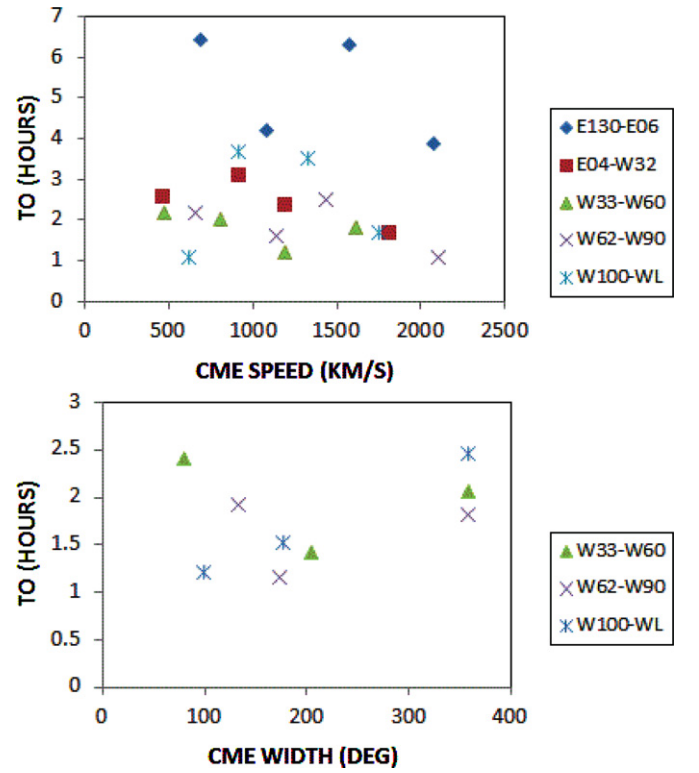

Figure 1. Top: plot of SEP event onset time TO medians vs. CME speed medians for the five longitude ranges. SEP events in each longitude range are divided into four speed groups of about 11 events in each speed group. Bottom: plot of SEP event TO medians vs. CME width medians for three western longitude ranges. SEP events in each longitude range are divided into three width groups, of which one group is exclusively 360° halo events.

(A color version of this figure is available in the online journal.)
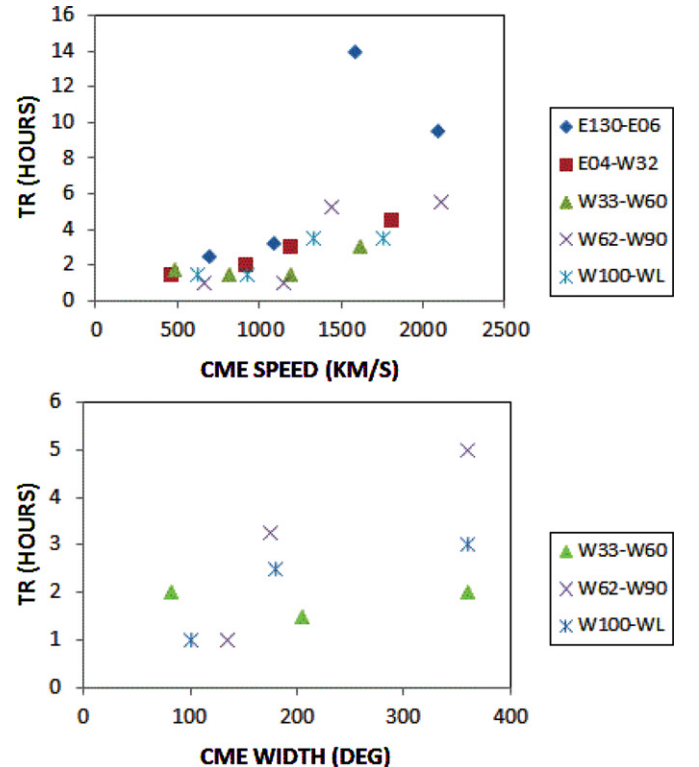
Figure 2. Same as Figure 1, but for the rise time TR medians.
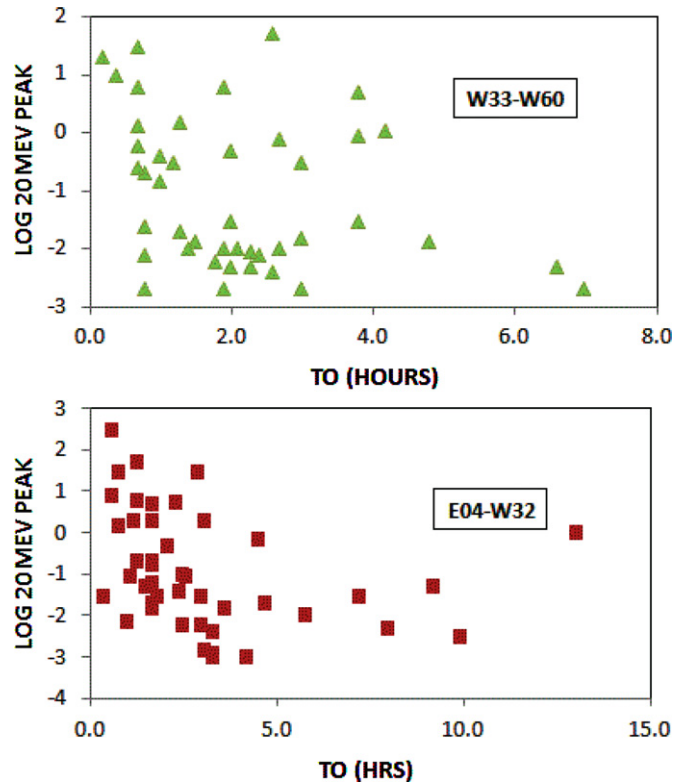(A color version of this figure is available in the online journal.)
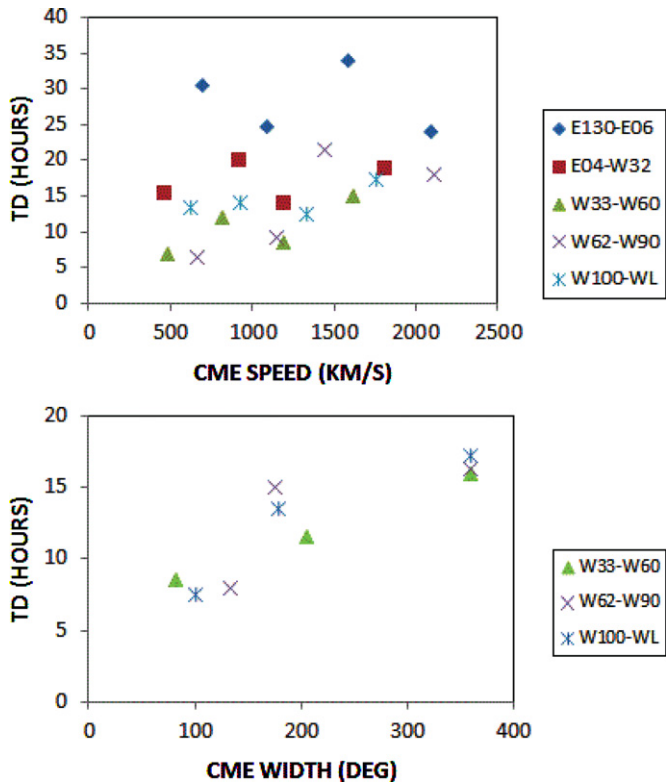
Figure 3. Same as Figure 1, but for the duration time TD medians.
(A color version of this figure is available in the online journal.)

Figure 4. Log plots of SEP event 20 MeV peak intensities vs. onset times TO for the W33°–W60° (top) and E04°–W32° (bottom) longitude ranges, showing the population of small SEP events with large (>4 hr) TO.
(A color version of this figure is available in the online journal.)

least subject to projection effects in the plane of the sky. In this case, the large number of 360° halo events in each longitude range suggests the use of only three width groups, the largest of which is only the halo events. The median TO, TR, and TD group values are plotted in the bottom panels of Figures 1–3, and the CCs for each longitude range are given in the middle part of Table 2. TR and TD are both correlated with W at CCs at or slightly below our CC $\geqslant 0.35$ significance criterion.

When we find an SEP event parameter, in this case TR or TD, that correlates with both v_{CME} and W, we have to be careful to check for a possible correlation between v_{CME} and W. This situation was first encountered for log Ip of SEP events by Kahler et al. (1984), who found that v_{CME} and W of the *Solwind/P-78* CMEs, each correlated with the associated SEP event log Ip, were not themselves correlated. On that basis, those authors concluded that v_{CME} and W were each somehow causal factors in SEP events. A recent comparison of 379 LASCO limb CMEs (Gopalswamy et al. 2009), however, has shown a strong linear correlation (CC = 0.69) between v_{CME} and W. A similar pair of CME width and speed correlations was presented in Figure 10 of Cane et al. (2010). For the 130 events of our W33°–WL longitude ranges v_{CME} and W are also correlated at CC = 0.46, well exceeding our 98% significance criterion. This immediately raises the question of whether only one of these variables is causally related to TR and TD, and if so, which?

2.5. SEP Peak Intensity Effects on Timescales

As discussed above, following numerous studies relating SEP peak intensities to CME properties, the goal here is to consider the SEP event timescales as a complementary tool for space weather forecasting and SEP physics. Implicit in K05 and the approach taken here is the assumption that the SEP
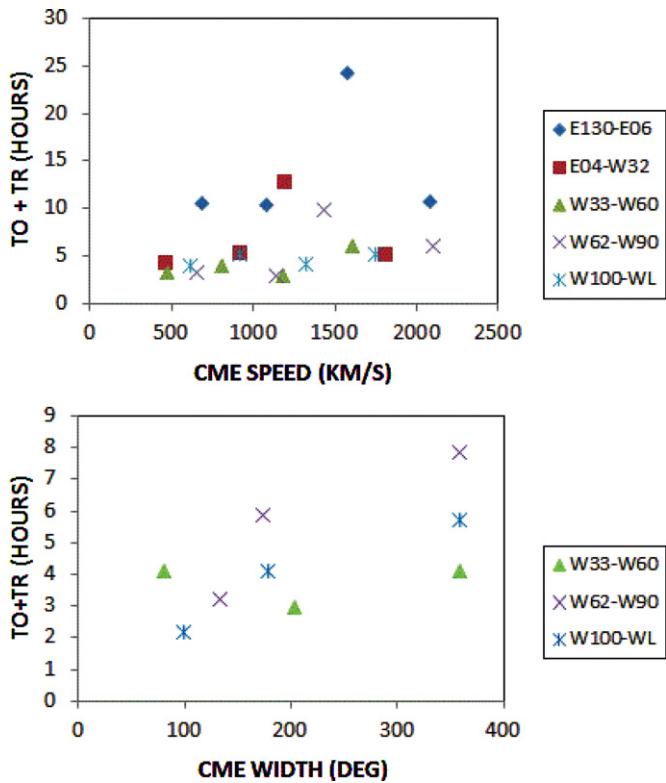
event timescales are independent of the associated SEP peak intensities Ip. Our definition of TR and TD, keyed to $0.5I$p, is intended to yield timescales independent of Ip. The parameter TO, however, does depend on the ratio of the SEP peak intensity to the background, as some studies and models have shown (Lintunen & Vainio 2004; Sáiz et al. 2005; Rouillard et al. 2012). In several cases the SEP event onsets of Table 1 occurred during the enhanced backgrounds of previous SEP events. We therefore qualitatively expect TO to be generally larger (later onsets) for smaller SEP events, which in turn implies smaller TR for smaller SEP events. These effects should produce negative (positive) CCs for TO (TR) with log Ip.

We plotted log Ip versus TO and TR and calculated the corresponding CCs, which are presented in the bottom section of Table 2. The expected correlations are found, and the significant CCs are italicized, this time with a lower threshold of CC $\geqslant 0.25$, appropriate for 90% significance for 44 events. We employ the lower 90% threshold here since we look for an expected bias in the SEP timescale determinations, rather than for physical relationships with CMEs, as we did above. We show plots of two of the four significantly correlated longitude ranges of TO in Figure 4. The plots illustrate the five orders of magnitude spanned by Ip and how the TO distributions are skewed to smaller values for larger Ip. The main drivers of the negative correlations appear to be the small Ip events with TO > 4 hr in each plot. Inspection of those events in Figure 4 shows, however, that backgrounds of only 5 of the total 13 events exceeded the median 20 MeV background value of 0.0005 p cm^{-2} s^{-1} sr^{-1} MeV^{-1}. Furthermore, the 13 events include none of the 6 or 7 impulsive SEP events of Reames & Ng (2004) included in Table 1. Thus, while background effects

Figure 5. Same as Figure 1, but for the combined onset and rise time (TO+TD) medians.

(A color version of this figure is available in the online journal.)

Table 3
Median Timescales[a] of SEP Events

Longitude	TO	TR	TD	TO+TR
E130°–E06°	6.2	8.5	26.0	14.3
E04°–W32°	2.4	2.0	17.5	4.9
W33°–W60°	1.9	2.0	12.0	3.9
W62°–W90°	1.7	2.5	12.0	5.1
W100°–WL	1.9	2.3	14.0	4.5

Note. [a] Units of hours.

3. DISCUSSION

We have looked for correlations of 20 MeV SEP event timescales with CME speeds v_{CME} and widths W using a data set of 217 SEP events over the 1996–2008 period. This study, revised and extended from our previous K05 study, considers the correlation variations with source longitudes and is complementary to works relating SEP peak intensities Ip to CME properties. The CME v_{CME} was generally correlated with TR (Figure 2 and Table 2). This result is consistent with the correlation of SEP rise times (onset to peak) with v_{CME} found by Hwang et al. (2010) for a sample of 63 GOES $E >$ 10 MeV proton events. Their CC = 0.34 is similar to our CC = 0.28 taking all 217 events together. TD correlates with v_{CME} in the well-connected longitude ranges, consistent with the view that faster CMEs continue injecting SEPs over longer time periods.

The TR and TD timescales correlate with the CME width W, at or somewhat less than our 98% confidence level. We noted that this result is deduced for only the three western longitude ranges and that there are significant correlations between CME W and v_{CME} in those ranges (CC = 0.46) which could explain the timescale–W correlations as only a consequence of the W–v_{CME} correlation alone. However, Kahler & Gopalswamy (2009) make a connection between the general observed requirement of fast ($v_{CME} > 900$ km s^{-1}) and wide ($W > 60°$) CMEs for SEP event associations (Gopalswamy et al. 2008) and the fundamental difference between bow shocks and piston-driven shocks. Fast and narrow CMEs act as projectiles through the solar wind to produce only narrow bow shocks, but fast and wide CMEs drive broad piston-driven shocks as they accrete solar wind material ahead of themselves (Vršnak & Cliver 2008), even when v_{CME} may be subsonic. The interpretation we favor here for the W correlation with TR and TD is that a larger W implies a longer continued magnetic connection of the Earth to the SEP-producing regions of the broader piston-driven shock. In our view, both v_{CME} and W are contributing factors to the enhanced values of TR and TD. However, the general correlation of CME W with v_{CME} (Gopalswamy et al. 2009) does not allow us to preclude the third possibility that only W, and not v_{CME}, is the primary causal factor of longer correlated TR and TD.

A new aspect of this study is the relationship between the observed SEP timescales and peak intensities Ip. This was prompted by the previous work cited in Section 2.5 to model variations of SEP onset times observed at 1 AU as functions of solar injection profiles and ambient backgrounds. We found the statistically expected qualitative effects of larger TO (Figure 4) and slightly smaller TR for smaller peak intensities Ip. However, it is not clear that the population of small SEP events with TO $\geqslant$ 4 hr is necessarily due to the background effect since most of those events we examined in detail had relatively low

must contribute to the negative correlation and some incorrect CME associations are always possible, there may be a small population of SEP events with intrinsically large (>4 hr) TO values.

The way to finesse the expected threshold bias in TO and TR is simply to introduce TO+TR as a parameter, since the times of CME launch and of 0.5Ip are background independent. The last column of Table 2 gives those correlations, which for v_{CME} are positive but not significant. The correlations with W are positive for the three longitude ranges, but barely significant for only one range. The corresponding plots are shown in Figure 5.

With TD and the more robust parameter TO+TR we can now ask whether those 20 MeV SEP timescales are independent of log Ip. The CCs of the last two columns of the bottom section of Table 2 show that result. The negative correlations with TO and positive with TR now essentially disappear with the small CCs for TO+TR. There is a trend, however, for TD to increase with log Ip for well-connected (W33°–W60°) events but to decrease with more poorly connected events.

2.6. Median SEP Timescales by Longitude

Determining the median timescales of the SEP events is a secondary goal of this work, and those times are given in Table 3. Since most of the SEP events of this study were included in K05, the median timescales of the five longitude ranges of Table 3 are only slightly changed from those of comparable longitude ranges in Table 2 of K05. There is a clear trend for timescales to increase from well-connected longitude (W33°–W90°) ranges toward the limbs. As emphasized above, the scatter in those parameters is considerable, as can be seen by comparing the TO values of the W33°–W60° and E04°–W32° events in Figure 1 with their corresponding distributions of Figure 4.

backgrounds. We also note that the background variations of the SEP onset models produced differences of minutes to several tens of minutes at most in their onset times. Here we deal with half-hour averages of SEP intensities, a much coarser time bin than considered in the models. An implication is that the weak inverse correlations of TO with v_{CME} shown in the first column of Table 2 and in the top of Figure 1 are negligibly biased by a possible background effect.

Large intensity SEP events tend to have long durations, and we looked for any correlation between TD, defined as the time the SEP intensity remains within $0.5I$p, and Ip itself. The results in Table 2 suggest a tendency for broader SEP intensity peaks with larger Ip at well connected but not poorly connected longitudes. However, TO+TR, the time from CME launch to the time of $0.5I$p, is independent of Ip. The well-known correlation of SEP log Ip with CME speed v_{CME} and width W therefore does not imply any relationship of SEP timescales with those CME parameters. They must be separately investigated, as we have done here.

The TR values can be compared roughly to ΔT_m, the time from onset to maximum, of 20–80 MeV protons of Figure 13 of van Hollebeke et al. (1975). At central and western longitudes, our TR values are somewhat smaller than those of ΔT_m, as expected, since ΔT_m extends from SEP onset to the full Ip. However, for eastern hemisphere events our TR value of 8.5 hr appears less than the fitted value for ΔT_m. Cane et al. (1988) analyzed a comparable sample of 235 SEP events with delays from Hα flare maximum to time of Ip, comparable to our TO+TR. Here again, looking at $E = 43$–81 MeV events of their Figure 8, we find good agreement for western events, but much lower TO+TR for our central and eastern events, despite our lower 20 MeV energy range. The significantly longer rise timescales of the eastern hemisphere events of van Hollebeke et al. (1975) and Cane et al. (1988) are likely due not only to our times of $0.5I$p versus their Ip times, but also to their including peak intensities at times of shocks for many of their events, while we base TR on the peak observed well before any later shock peak. We conclude that our timescale results are compatible with those earlier works.

A final goal was to provide better timescales of $\sim$20 MeV SEP events to aid in space weather forecasting. Given an observed CME speed or width and/or an X-ray or Hα flare, Figures 10 and 11 of Cane et al. (2010) show the ranges of subsequent associated peak SEP intensities Ip. Our Figures 1–3 show the complementary median timescales as functions of CME speeds and widths for five source longitude ranges. Those timescales are presented as median values of $\sim$44 events per longitude range in Table 3 and are similar to the corresponding timescales of Table 2 of K05, as expected from the many SEP events common to both data sets. All the timescales reach minimal values in the best connected longitude ranges. With these studies comes the caveat that we and Cane et al. (2010) do not consider those cases in which fast and wide CMEs may not result in any observed SEP events, so SEP event probabilities can not be deduced from these studies.

REFERENCES

Balch, C. C. 1999, Rad. Meas., 30, 231
Bevington, P. R., & Robinson, D. K. 2003, Data Reduction and Error Analysis for the Physical Sciences (New York: McGraw-Hill)
Burkepile, J. T., Hundhausen, A. J., Stanger, A. L., St. Cyr, O. C., & Seiden, J. A. 2004, JGRA, 109, A03103
Cane, H. V., Mewaldt, R. A., Cohen, C. M. S., & von Rosenvinge, T. T. 2006, JGRA, 111, A06S90
Cane, H. V., Reames, D. V., & von Rosenvinge, T. T. 1988, JGR, 93, 9555
Cane, H. V., Richardson, I. G., & von Rosenvinge, T. T. 2010, JGRA, 115, A08101
Cliver, E. W., & Ling, A. G. 2007, ApJ, 658, 1349
Desai, M. I., Mason, G. M., Gold, R. E., et al. 2006, ApJ, 649, 470
Gopalswamy, N., Dal Lago, A., Yashiro, S., & Akiyama, S. 2009, CEAB, 33, 115
Gopalswamy, N., Xie, H., Makela, P., et al. 2010, ApJ, 710, 1111
Gopalswamy, N., Yashiro, S., Akiyama, S., et al. 2008, AnGeo, 26, 3033
Gopalswamy, N., Yashiro, S., Krucker, S., Stenborg, G., & Howard, R.A. 2004, JGRA, 109, A12105
Harrison, R. 2006, in Solar Eruptions and Energetic Particles, Vol. 165, ed. N. Gopalswamy, R. Mewaldt, & J. Torsti (Washington, D.C.: AGU), 73
Hwang, J., Cho, K.-S., Moon, Y.-J., Kim, R.-S., & Park, Y.-D. 2010, AcAau, 67, 353
Kahler, S. W. 2005, ApJ, 628, 1014
Kahler, S. W. 2008, in Proc. 30th Int. Cosmic Ray Conf. (Merida), Vol. 1, ed. R. Caballero et al. (Mexico City: Universidad Nacional Autonoma de Mexico), 143
Kahler, S., & Gopalswamy, N. 2009, Proc. 31st Int. Cosmic Ray Conf., http://icrc2009.uni.lodz.pl/proc/pdf/icrc0266.pdf
Kahler, S. W., Reames, D. V., & Sheeley, N. R., Jr. 2001, ApJ, 562, 558
Kahler, S. W., Sheeley, N. R., Jr., Howard, R. A., et al. 1984, JGR, 89, 9683
Krucker, S., White, S. M., & Lin, R. P. 2007, ApJL, 669, L49
Kumar, S., Janki, P., & Raizada, A. 2009, Indian J. Radio Space Phys., 38, 129
Lintunen, J., & Vainio, R. 2004, A&A, 420, 343
Pan, Z. H., Wang, C. B., Wang, Y., & Xue, X. H. 2011, SoPh, 270, 593
Park, J., Moon, Y.-J., & Gopalswamy, N. 2012, JGRA, 117, A08108
Reames, D. V. 1999, SSRv, 90, 413
Reames, D. V. 2013, SSRv, in press
Reames, D. V., & Ng, C. K. 2004, ApJ, 610, 510
Reinard, A. A., & Andrews, M. A. 2006, AdSpR, 38, 480
Rouillard, A. P., Sheeley, N. R., Jr., Tylka, A., et al. 2012, ApJ, 752, 44
Sáiz, A., Evenson, P., Ruffolo, D., & Bieber, J. W. 2005, ApJ, 626, 1131
van Hollebeke, M. A. I., Ma Sung, L. S., & McDonald, F. B. 1975, SoPh, 41, 189
Vršnak, B., & Cliver, E. W. 2008, SoPh, 253, 215
Wang, R. 2006, Aph, 26, 202
Xue, X. H., Wang, C. B., & Dou, X. K. 2005, JGRA, 110, A08103
Yashiro, S., & Gopalswamy, N. 2009, in IAU Symp. 257, Universal Heliospheric Processes, ed. N. Gopalswamy & D. F. Webb (Cambridge: Cambridge Univ. Press), 233